Electronic Supplementary Information (ESI)

ESI Mass spectrometry.

The general ESI source parameters optimized for each complexes' analysis were as follows: **L1**-H**L3**. Positive polarity, Ionspray Voltage Floating 5500 V, Temperature 0, Ion source Gas 1 (GS1) 20 L/min; Ion source Gas 2 (GS2) 0; Curtain Gas (CUR) 15 L/min, Collision Energy (CE) 10 V; Declustering Potential (DP) 100 V, range 120-600 m/z. H**L2**. Positive polarity, Ionspray Voltage Floating 5500 V, Temperature 0, Ion source Gas 1 (GS1) 20 L/min; Ion source Gas 2 (GS2) 0; Curtain Gas (CUR) 25 L/min, Collision Energy (CE) 10 V; Declustering Potential (DP) 150 V, range 120-800 m/z. For acquisition, Analyst TF software 1.7.1 (Sciex) was used and deconvoluted spectra were obtained by using the Bio Tool Kit micro-application v.2.2 embedded in PeakView™ software v.2.2 (Sciex).

Single crystal X-ray diffraction analysis of $[(H_4L4)(ClO_4)_4]4H_2O$

Single crystal diffraction measurement for compound $[(H_4\mathbf{L4})(ClO_4)_4]\cdot 4H_2O$ was carried out with an Oxford Diffraction Excalibur diffractometer using the Mo-Kα radiation (λ = 0.71073 Å). Data collection was performed with the program CrysAlis CCD.[i] Data reduction was carried out with the program CrysAlis RED.[ii] Finally, absorption correction was performed with the program ABSPACK in CrysAlis RED.

The structure was solved by using the SIR-2004 package[iii] and subsequently refined on the F^2 values by the full-matrix least-squares program SHELXL-2013.[iv]

Geometrical calculations were performed by PARST97,[v] and molecular plots were produced by the programs ORTEP-3[vi], Mercury (v.3.7)[vii] and Discovery Studio Visualizer (v4.5).[viii]

In Table S1 crystal data and refinement parameters of $[(H_4\mathbf{L4})(ClO_4)_4]\cdot 4H_2O$ are reported. All the non-hydrogen atoms were anisotropically refined. The hydrogen atoms of the $H_4\mathbf{L4}^{4+}$ cation, with the exception of those bound to the nitrogen ones, were introduced in calculated position; while the four protonation hydrogen atoms, as well as the hydrogen atoms of the four water molecules, where found in the Fourier difference map and isotropically refined; their isotropic thermal parameters were set accordingly to those of the atoms to which they are bound.

Finally, in $[(H_4\mathbf{L4})(ClO_4)_4]\cdot_4(H_2O)$ one perchlorate anion is disordered. Such disorder was modelled by introducing double positions for the oxygen atoms of the anion, with an occupancy factor of 0.79 and 0.21, respectively.

In the asymmetric unit of $[(H_4\mathbf{L4})(ClO_4)_4]\cdot 4H_2O$ one $H_4\mathbf{L4}^{4+}$ cation, four perchlorate anions and four water molecules are present. In figure S20 an ORTEP-3 view of the cation is reported.

The cyclen base of the macrocycle takes the usual (for biprotonated cyclen rings)[ix] [3333]-C corner conformation with the distances between the opposite couple of nitrogen atoms of 4.025(6) and

4.210(7) Å for N(1)/N(3) and N(2)/N(4), respectively. The protonation hydrogen atoms bonded to N(2) and N(4), that point inside the macrocyclic cavity, weakly interact, *via* hydrogen bonds, with the other two nitrogen atoms N(1) and N(3) (see table S2).[x]

The two quinoline moieties lie on the same side with respect to the mean plane defined by the four nitrogen atoms of the macrocycle (A in the following, see Figure S21) and are quite parallel each other [the angle between the mean planes defined by the non-hydrogen atoms of the two moieties is 13.7(1)°] and parallel to the plane A (the angle between A and the plane defined by the non-hydrogen atoms of the two quinoline groups are 15.3(1) and 9.9(1)°). In the macrocyclic cavity is lodged one perchlorate anion that interact via hydrogen bonds with the two protonated nitrogen atoms (see Figure S22 and table S2).

In the crystal packing of $[(H_4\mathbf{L4})(ClO_4)_4]\cdot 4H_2O$, $H_4\mathbf{L4}^{4+}$ cations are held together by π-π interactions involving the C(10)-C(18) quinoline group and the symmetry related (x-1, y,z) C(20)-C(28) one (the angle between the mean planes defined by the non-hydrogen atoms of the two groups is 13.73(9)° while the distance between the two quinoline centroids is 3.853(8) Å). As a consequence, the $H_4\mathbf{L4}^{4+}$ cations arrange themselves in ribbons along the a axis (see figure S23) which are connected by a net of strong hydrogen bonds (see table 2) that involves the perchlorate anions and water molecules.

Finally, in the Cambridge Structural database (CSD, v. 5.37)[9] were retrieved six molecules similar to the $H_4\mathbf{L4}^{4+}$ cation (see scheme S1).

Of these two (refcodes = HAVFEP[xi] and SELGAT[xii]) have an open disposition of the two side-arms very similar to that observed in $[(H_4\mathbf{L4})(ClO_4)_4]4\cdot H_2O$ (see figure S24). Interestingly in both compounds, as already observed in$[(H_4\mathbf{L4})(ClO_4)_4]\cdot 4H_2O$ (see above), due to the fact that there are no groups in the side-arms able to interact *via* hydrogen bonds with the protonated nitrogen atoms of the macrocyclic base, an external species (*i.e.* ClO_4^- in $[(H_4\mathbf{L4})(ClO_4)_4]\cdot 4H_2O$ and SELGAT, Br^- in HAVFEP) enters the inner cavity of the ligand and interacts with them. On the contrary, in the other four molecules[xiii] a net of strong hydrogen bonds involving the protonated nitrogen atoms of the base and acceptor groups located on the side arms is present (see figure S25).

Determination of fluorescence quantum yields of compounds

Fluorescence quantum yields (Φ, uncertainty ± 15%) of the receptors, shown in Table S3, were determined by comparing the integrated fluorescence spectra of the samples with a solution of Quinine sulfate in H_2SO_4 as a reference (0.05 M; Φ = 0.53), accordingly to methods reported in literature.[IV] The given formula was used for the determination of quantum yield values:

$$\Phi = \Phi_r \frac{I\, A_r\, n^2}{I_r\, A\, n_r^2}$$

where Φ is the quantum yield, I is the integrated emission intensity, A is the absorbance at the excitation wavelength, and n is the refractive index of the solvent. The subscript r refers to the reference fluorophore of known quantum yield.

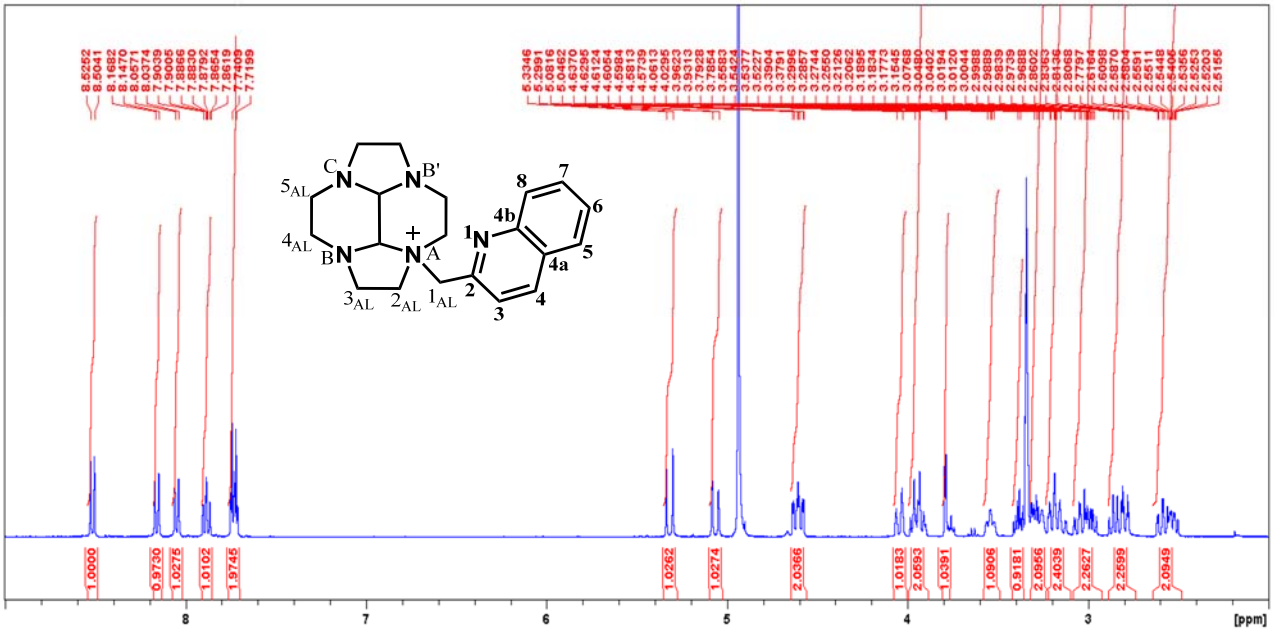

Fig. S1. ^{1}H NMR spectra of compound **4** (MeOD, 400 MHz): δ(ppm) 8.52 (d, 1H, J=8.44 Hz, H8), 8.16 (d, 1H, J=8.48 Hz, H4), 8.05 (d, 1H, J=8 Hz, H5), 7.88 (t, 1H, J=8.04 Hz, H7), 7.75-7.70 (m, 2H, H6, H3), 5.32 (d, 1H, J=14.2 Hz), 5.06 (d, 1H, J=14.2 Hz), 4.63-4.57 (m, 2H, 1_{AL}), 4.07-4.01 (m, 1H), 3.97-3.90 (m, 2H), 3.79-3.75 (m, 1H), 3.57-3.51 (m, 1H), 3.41-3.36 (m, 1H), 3.32-3.23 (m, 2H), 3.23-3.11 (m, 2H), 3.08-2.95 (m, 2H), 2.89-2.77 (m, 2H), 2.62-2.49 (m, 2H).

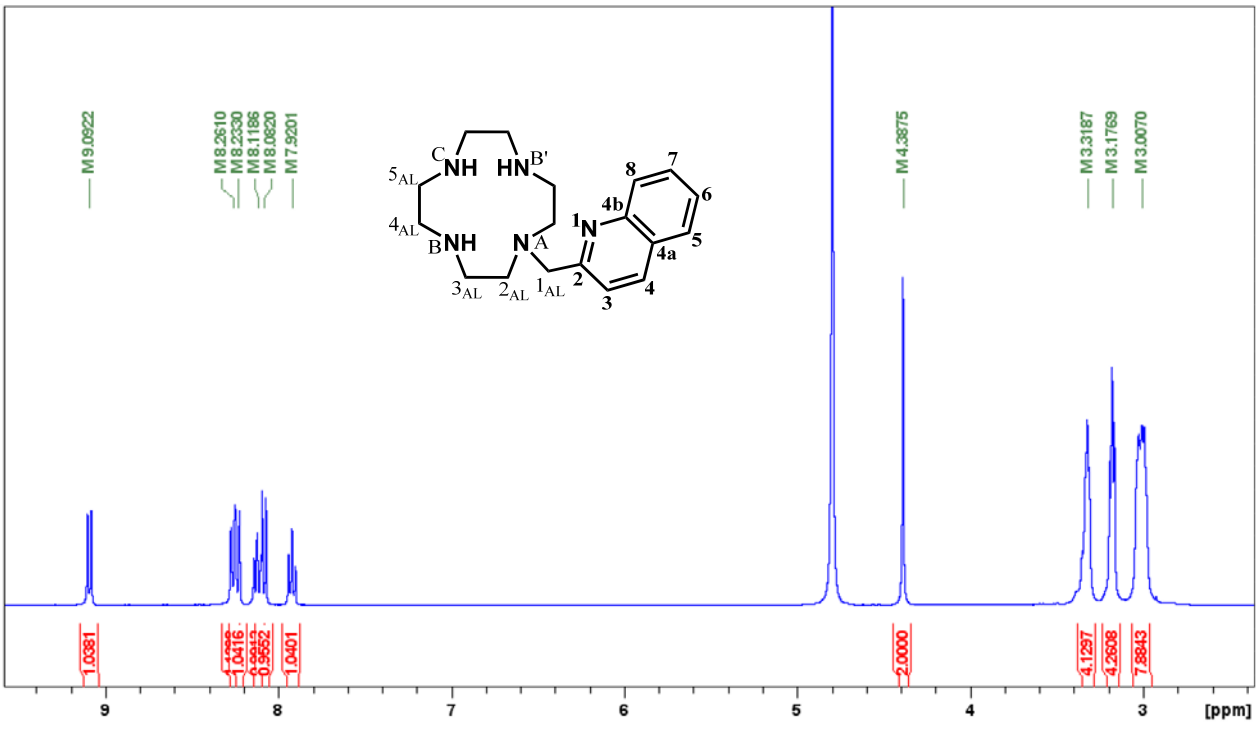

Fig. S2. ^{1}H NMR spectra of compound **L1** (D_2O, pD < 2, 400 MHz): δ(ppm) 9.09 (d, 1H, H8, J=8.5 MHz), 8.26 (d, 1H, H4, J=8.6 MHz), 8.23 (d, 1H, H5, J=9.1 MHz), 8.12 (t, 1H, H7, J=7.9 MHz), 8.08 (d, 1H, H3, J=8.6 MHz), 7.92 (t, 1H, H6, J=7.3 MHz), 4.38 (s, 2H, 1_{AL}), 3.33-3.31 (m, 4H), 3.17-3.16 (m, 4H), 3.03-2.98 (m, 8H).

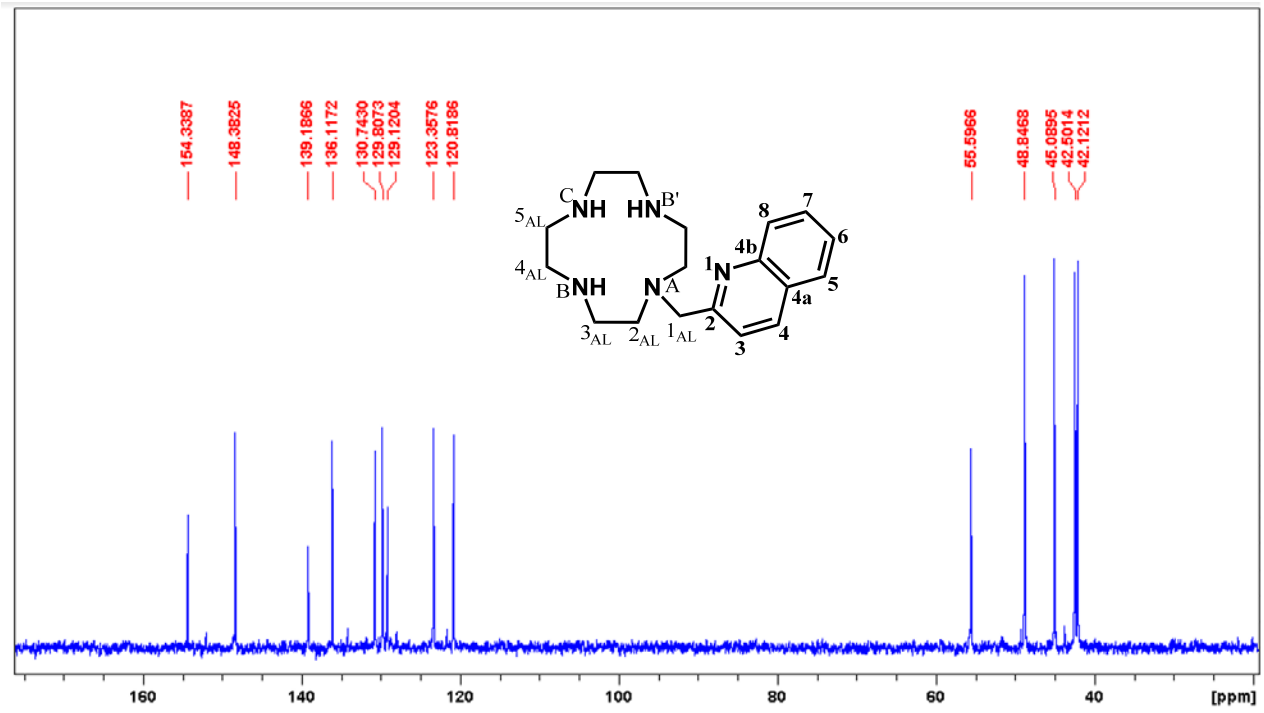

Fig. S3. ^{13}C NMR spectra of compound **L1** (D_2O, pD < 2, 400 MHz): δ(ppm) 154.34, 148.38, 139.19, 136.12, 130.74, 129.81, 129.12, 123.36, 120.82, 55.60, 48.85, 45.09, 42.50, 42.12.

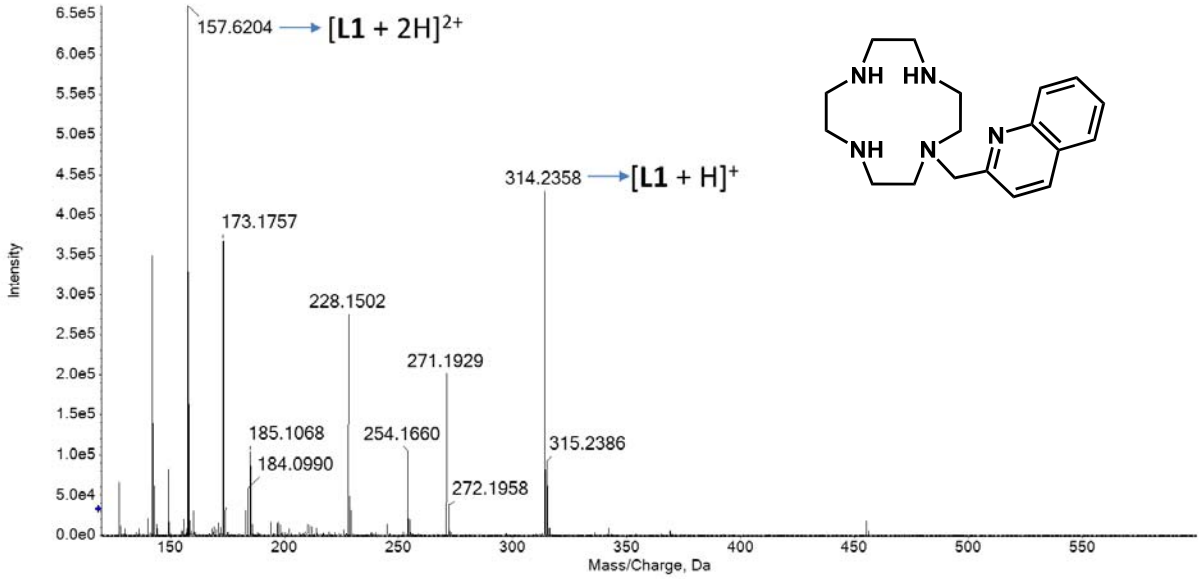

Fig. S4. High resolution mass spectrum of compound **L1** in H_2O; 314.236 (z = 1, [**L1** + H]$^+$); 157.620 (z = 2, [**L1** + 2H]$^{2+}$).

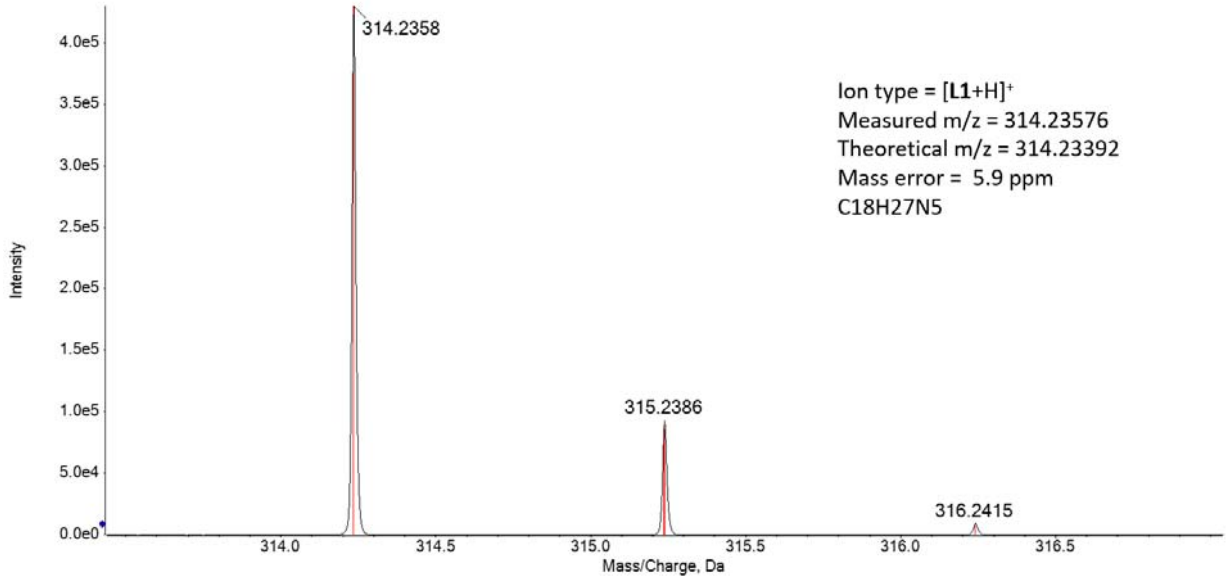

Fig. S5. Isotopic pattern of the [**L1**+H]$^{+}$ (Z = 1) ion, with measured (black) and theoretical (red) m/z value of the most abundant isotopic peak, 313.5-317 Da region.

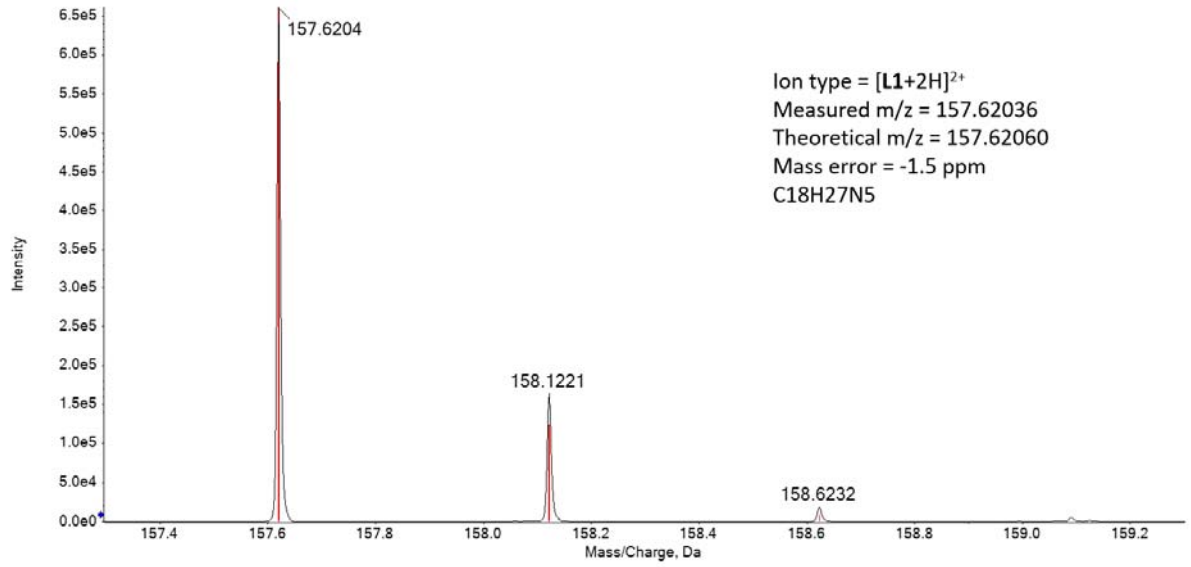

Fig. S6. Isotopic pattern of the [**L1**+2H]$^{2+}$ (Z = 2) ion, with measured (black) and theoretical (red) m/z value of the most abundant isotopic peak, 157.5-159.3 Da region.

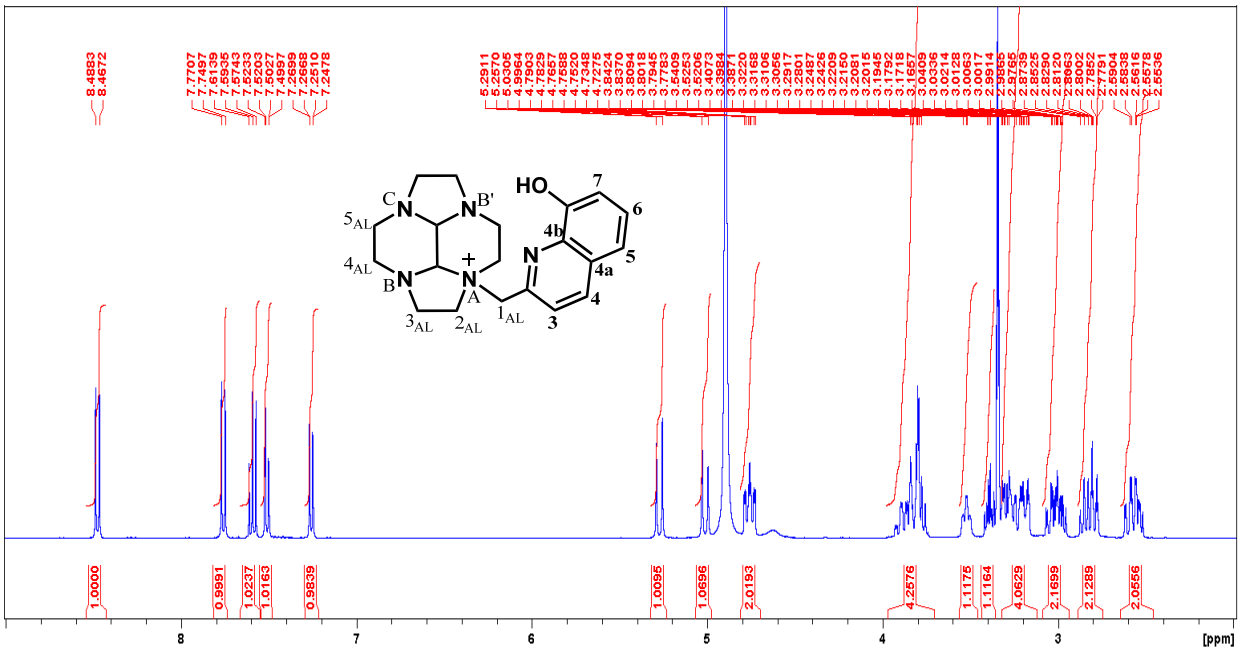

Fig. S7. ^{1}H NMR spectra of compound **5** (MeOD, 400 MHz): δ(ppm) 8.48 (d, 1H, J=8.44 Hz, H4), 7.77 (d, 1H, J=8.40 Hz, H3), 7.60 (t, 1H, J=8.16 Hz, H6), 7.51 (d, 1H, J=8 Hz, H5), 7.26 (d, 1H, J=7.9 Hz, H7), 5.27 (d, 1H, J=13.64 Hz), 5.01 (d, 1H, J=13.64 Hz), 4.81-4.71 (m, 2H, 1_{AL}), 3.94-3.74 (m, 2H), 3.57-3.48 (m, 1H), 3.43-3.35 (m, 1H), 3.32-3.16 (m, 4H), 3.08-2.95 (m, 2H), 2.88-2.76 (m, 2H), 2.65-2.51 (m, 2H).

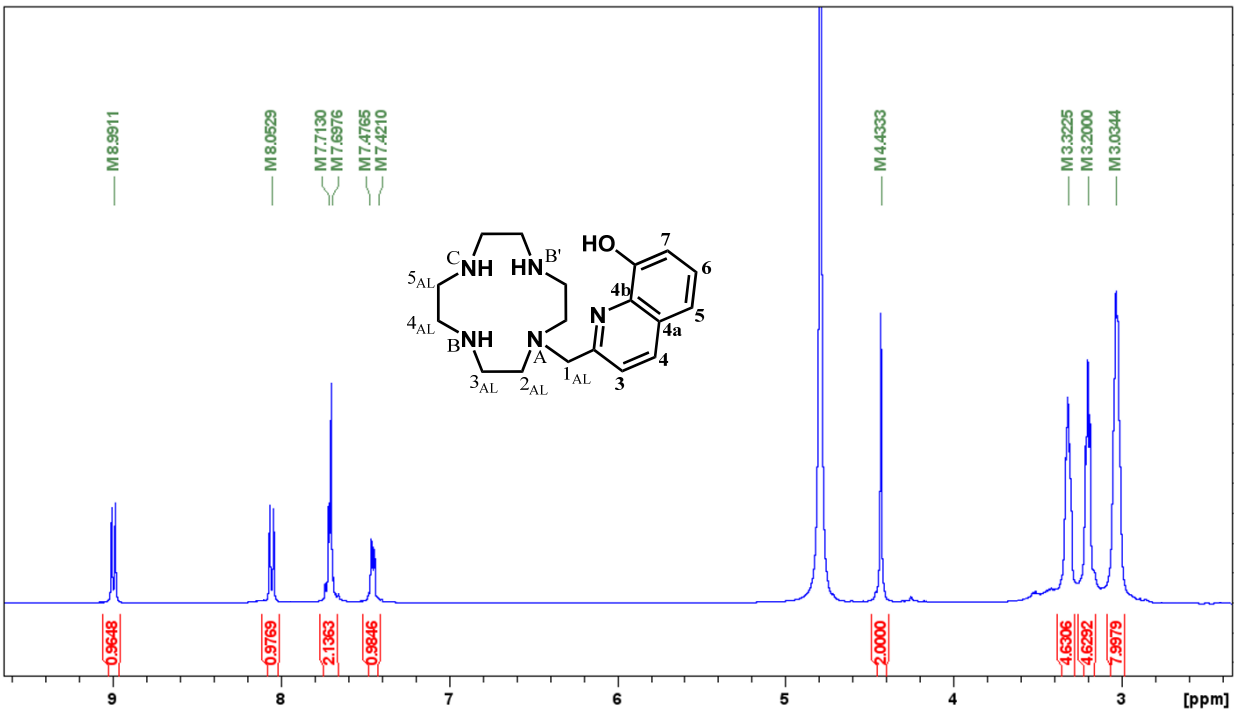

Fig. S8. ^{1}H NMR spectra of compound H**L2** (D_2O, pD < 2, 400 MHz): δ(ppm) 8.99 (d, 1H, H4, J=8.7 MHz), 8.05 (d, 1H, H3, J=8.6 MHz), 7.71-7.69 (m, 2H, H5, H6), 7.48-7.42 (d, 1H, H7), 4.43 (s, 2H, 1_{AL}), 3.36-3.28 (m, 4H), 3.24-3.17 (m, 4H), 3.08-2.99 (m, 8H).

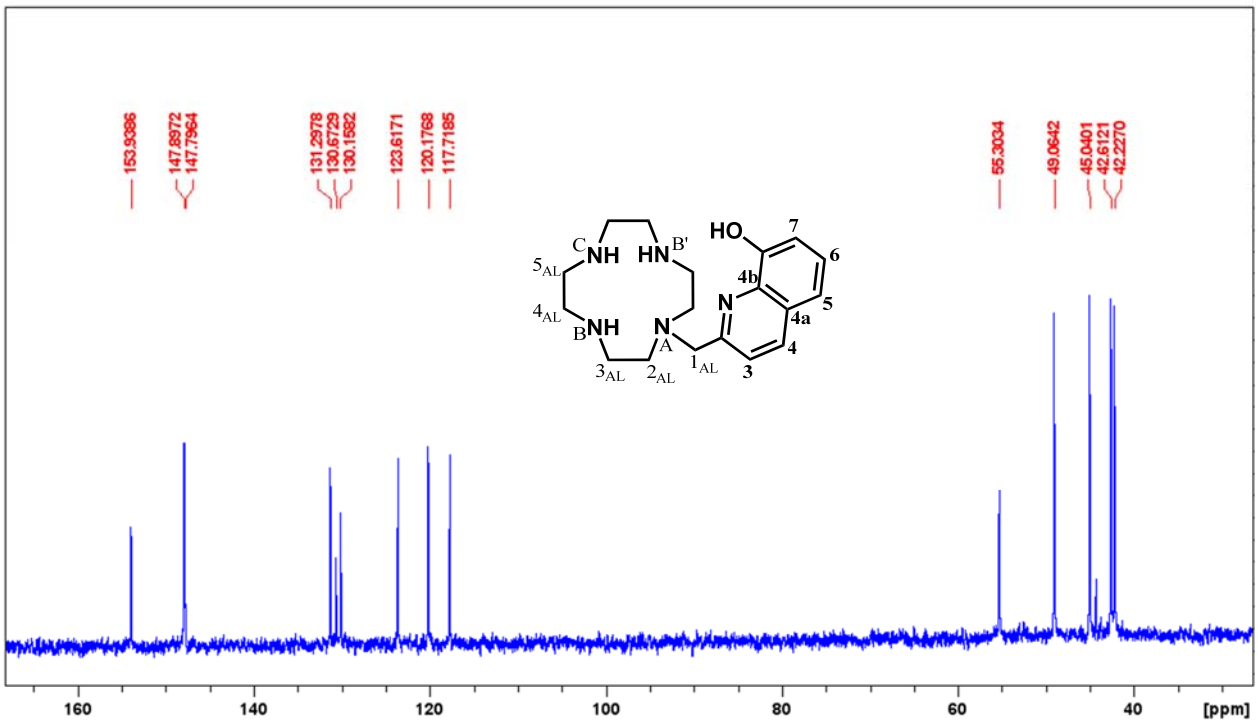

Fig. S9. ^{13}C NMR spectra of compound H**L2** (D_2O, pD < 2, 400 MHz): δ(ppm) 153.94, 147.90, 147.80, 131.30, 130.30, 130.16, 123.62, 120.18, 117.72, 55.30, 49.06, 45.04, 42.61, 42.23.

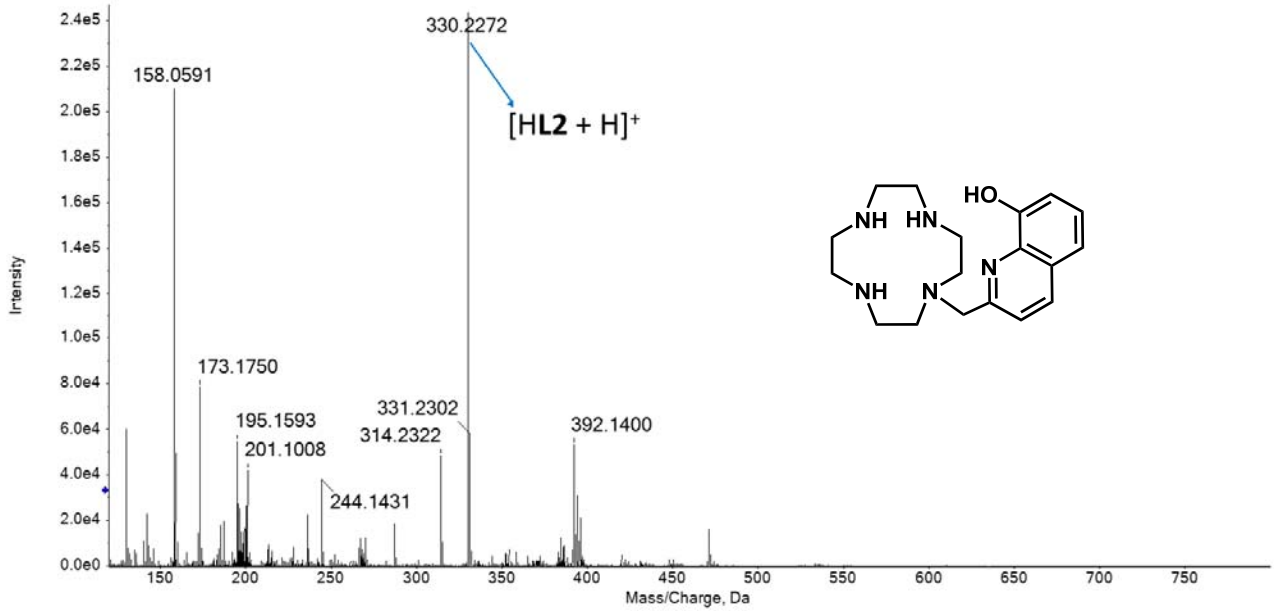

Fig. S10. High resolution mass spectrum of compound H**L2** in H_2O; 320.227 (z = 1, [H**L2** + H]$^+$).

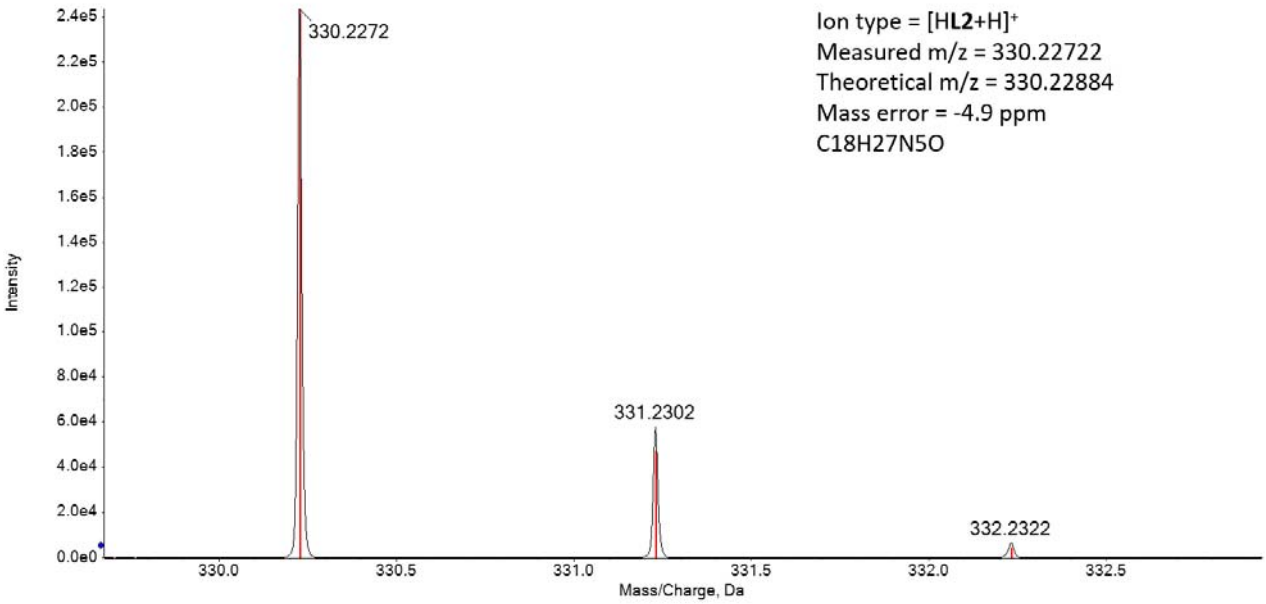

Fig. S11. Isotopic pattern of the [H**L2**+H]$^+$ (z = 1) ion, with measured (black) and theoretical (red) m/z value of the most abundant isotopic peak, 329.5-333 Da region.

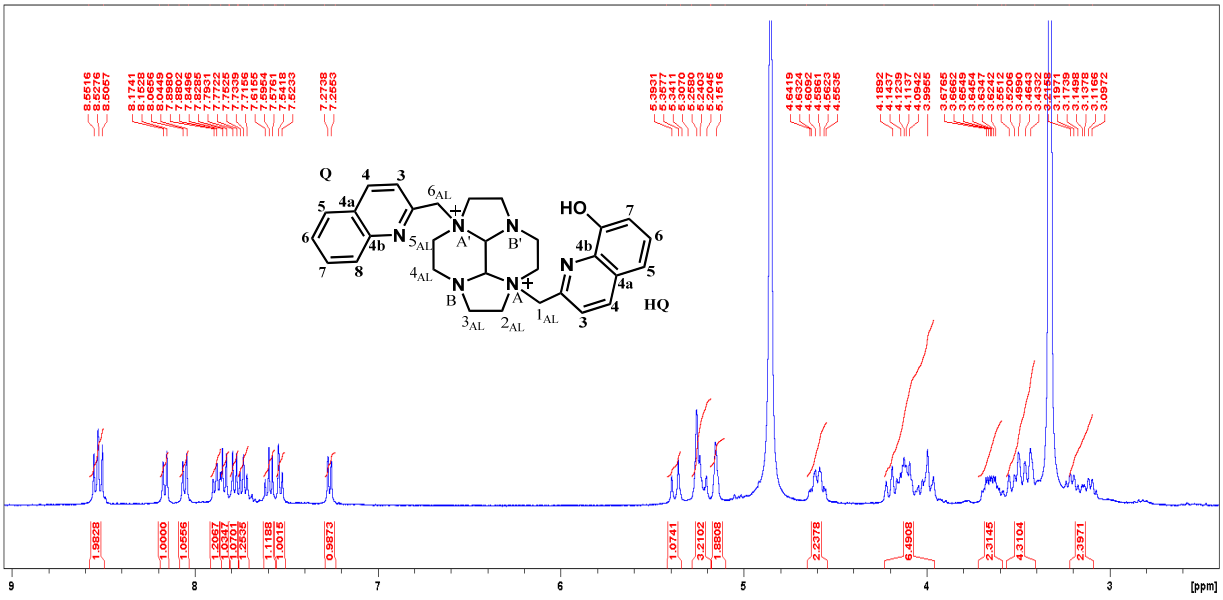

Fig. S12. ^{1}H NMR spectra of compound **6** (MeOD, 400 MHz): δ(ppm) 8.53 (m, 2H, J=9.6 Hz, H8(Q),H7(Q)), 8.17 (d, 1H, J=8.52 Hz, H4(HQ)), 8.06 (d, 1H, J=8.28 Hz, H4(Q)), 7.88 (d, 1H, J=7.12 Hz, H5(Q)), 7.84 (d, 1H, J=8.44 Hz, H3(HQ)), 7.78 (d, 1H, J=8.36 Hz, H3(Q)), 7.74 (t, 1H, J=7.32 Hz, H6(HQ)), 7.60 (t, 1H, J=8.04 Hz, H6(Q)), 7.53 (d, 1H, J=7.4 Hz, H5 (HQ)), 7.26 (d, 1H, J=7.4 Hz, H7(HQ)), 5.37 (d, 1H, J=14.16 Hz), 5.34 (m, 3H), 5.15 (s, 2H), 4.64-4.55 (m, 2H), 4.19-3.96 (m, 6H), 3.71-3.59 (m, 2H), 3.55-3.41 (m, 4H), 3.23-3.08 (m, 2H).

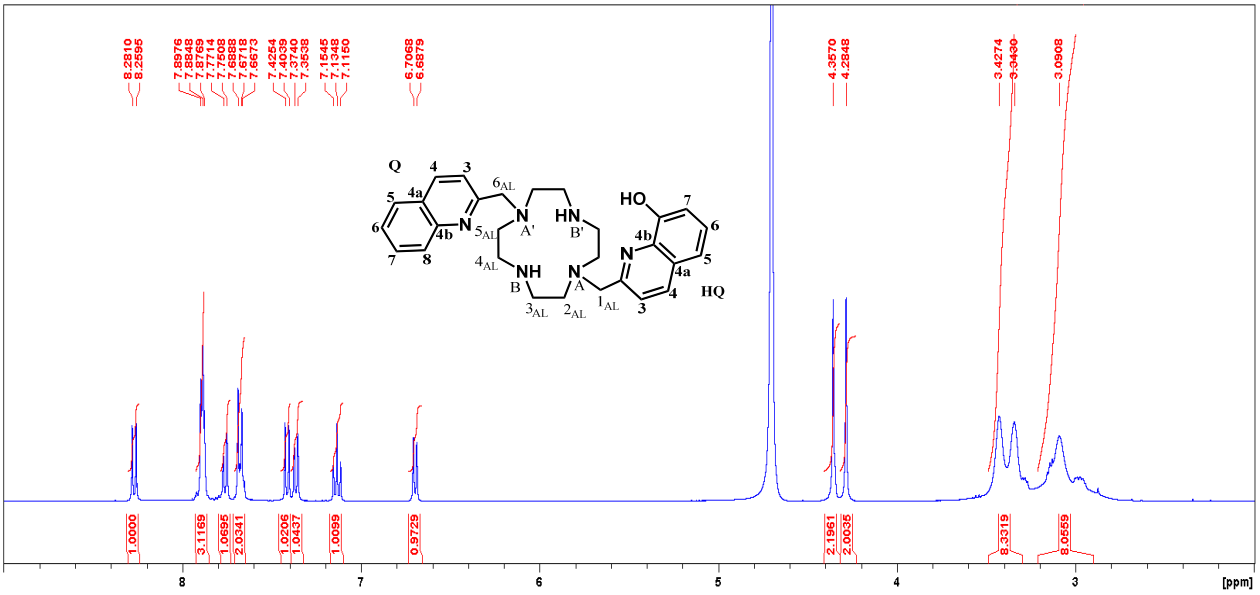

Fig. S13. ^{1}H NMR spectra of compound H**L3** (D_2O, pD < 2, 400 MHz): δ(ppm) 8.27 (d, 1H, J=8.6 Hz, H8(Q)), 7.89 (m, 3H, H7(Q), H4(HQ), H4(Q)), 7.77 (d, 1H, J=8.3 Hz, H3(HQ)), 7.68 (m, 2H, J=8.6 Hz, H6(HQ), H5(Q)), 7.42 (d, 1H, J=8.4 Hz, H5(HQ)), 7.37 (d, 1H, J=8.1 Hz, H3(Q)), 7.14 (t, 1H, J=7.90 Hz, H6(Q)), 6.70 (d, 1H, J=7.56 Hz, H7(HQ)), 4.36 (s, 2H), 4.28 (s, 2H), 3.50-3.26 (m 8H), 3.20-2.88 (m, 8H).

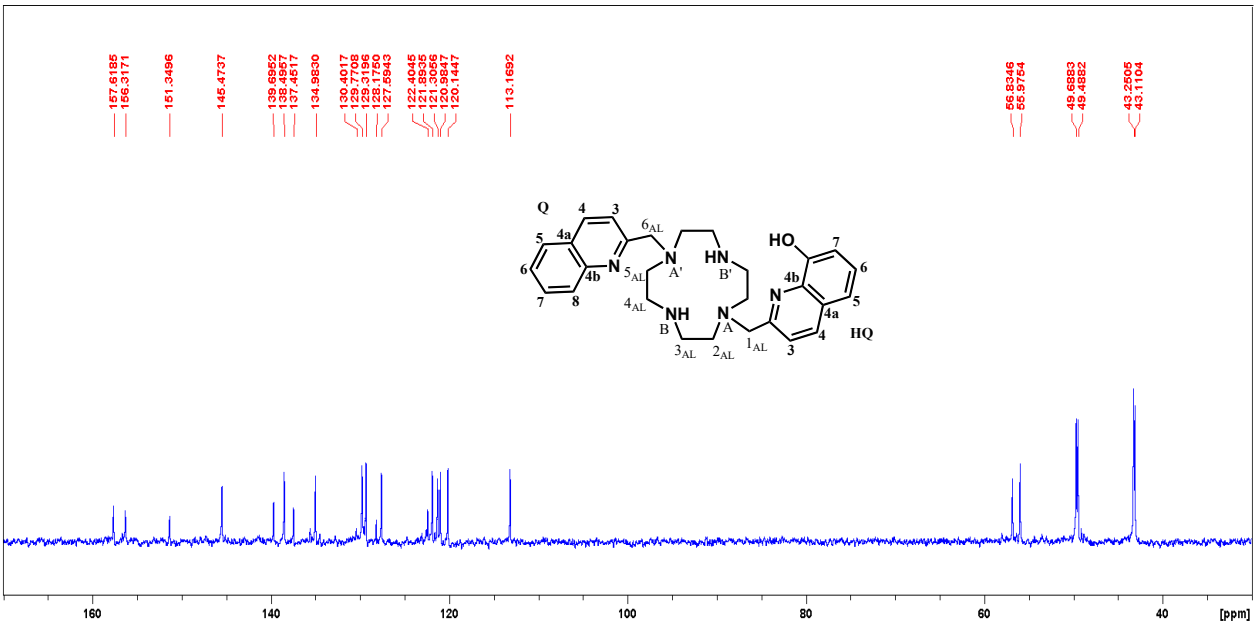

Fig. S14. ^{13}C NMR spectra of compound H**L3** (D_2O, pD < 2, 400 MHz): δ(ppm) 157.62, 156.31, 151.35, 145.47, 139.70, 138.50, 137.45, 134.98, 130.40, 129.77, 129.32, 128.18, 127.59, 122.40, 121.89, 121.31, 120.98, 120.14, 113.17, 56.83, 55.98, 49.69, 49.49, 43.25, 43.11.

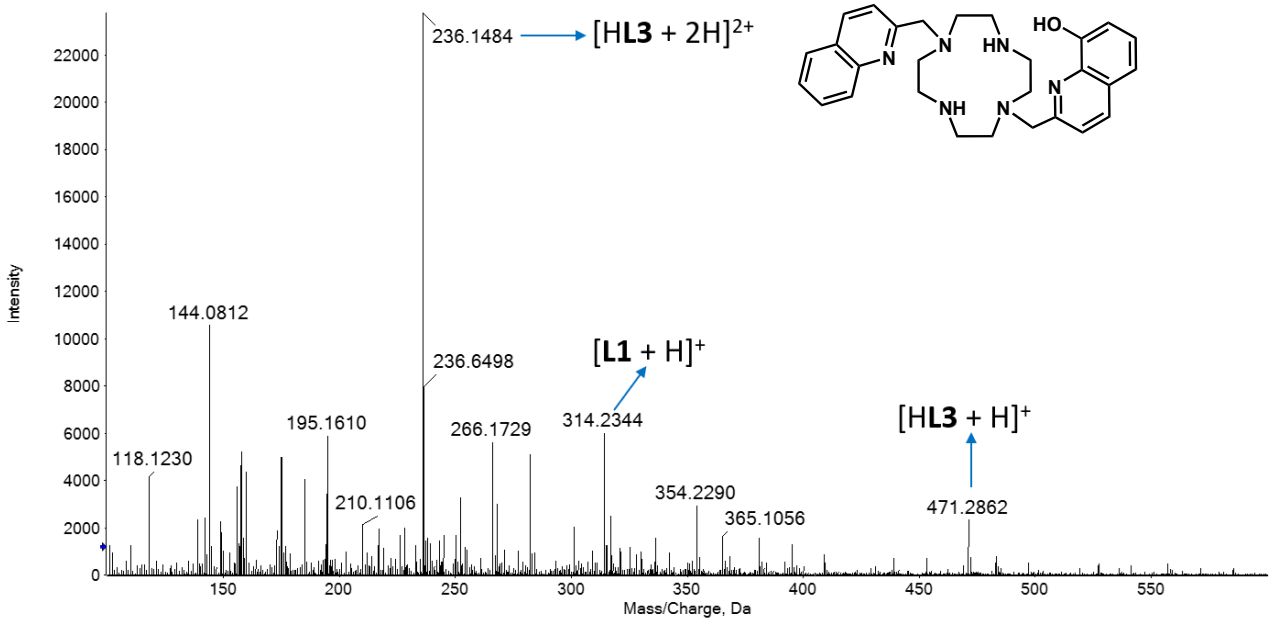

Fig. S15. High resolution mass spectrum of compound H**L3** in H_2O; 471.286 (z = 1, [H**L3** + H]$^+$); 236.1484 (z = 2, [H**L3** + 2H]$^{2+}$).The fragment [**L1** + H]$^+$ derives from the lost of a hydroxyquinoline unit from H**L3**.

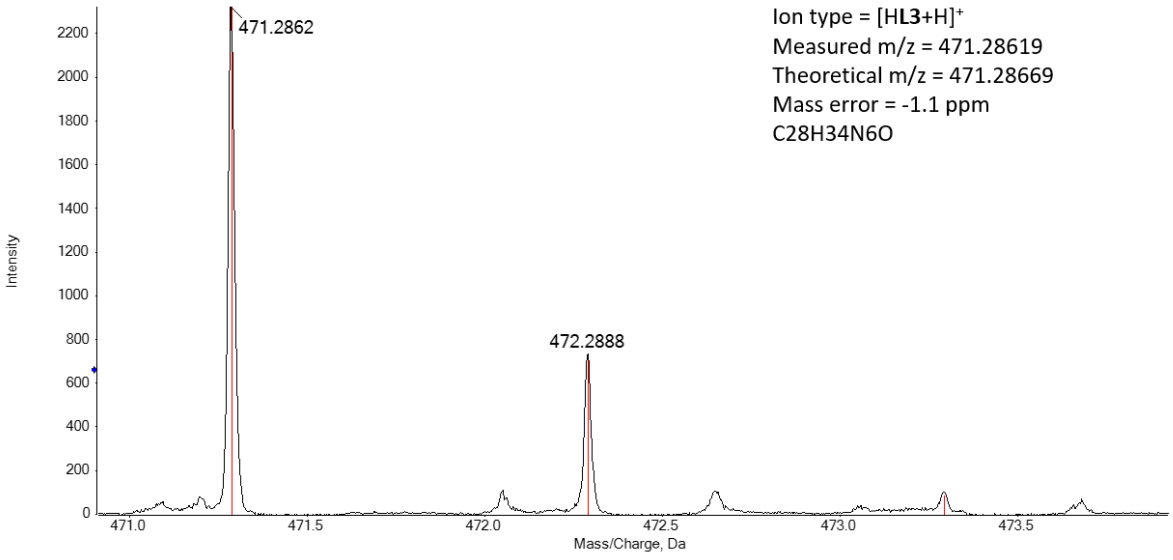

Fig. S16. Isotopic pattern of the [H**L3**+H]$^+$ (z = 1) ion, with measured (black) and theoretical (red) m/z value of the most abundant isotopic peak, 471-474 Da region.

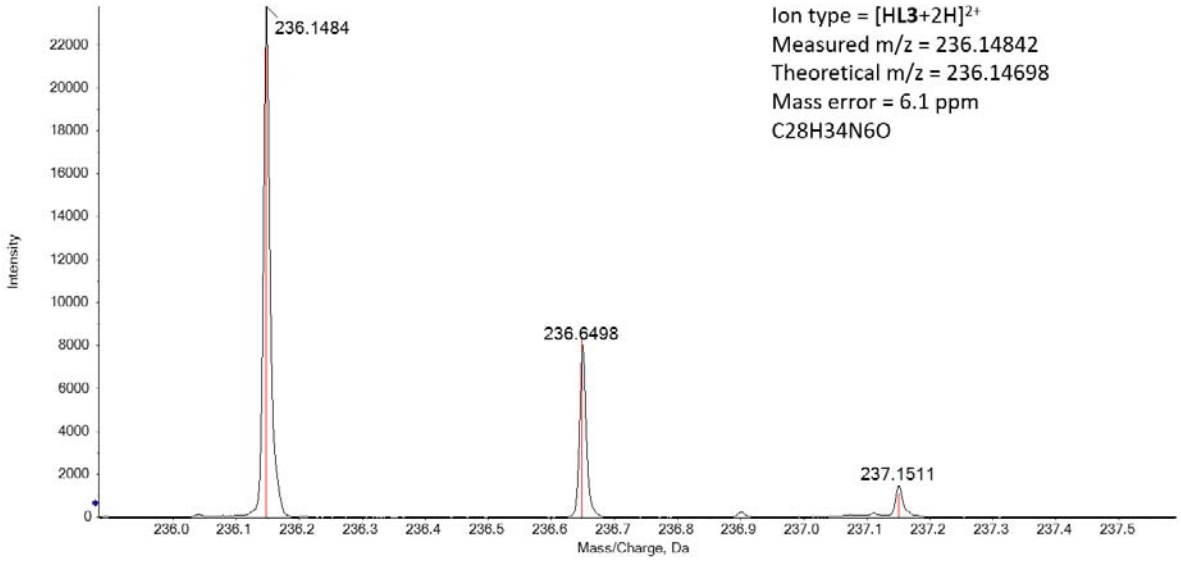

Fig. S17. Isotopic pattern of the [H**L3**+2H]$^{2+}$ (z = 2) ion, with measured (black) and theoretical (red) m/z value of the most abundant isotopic peak, 235.9-237.6 Da region.

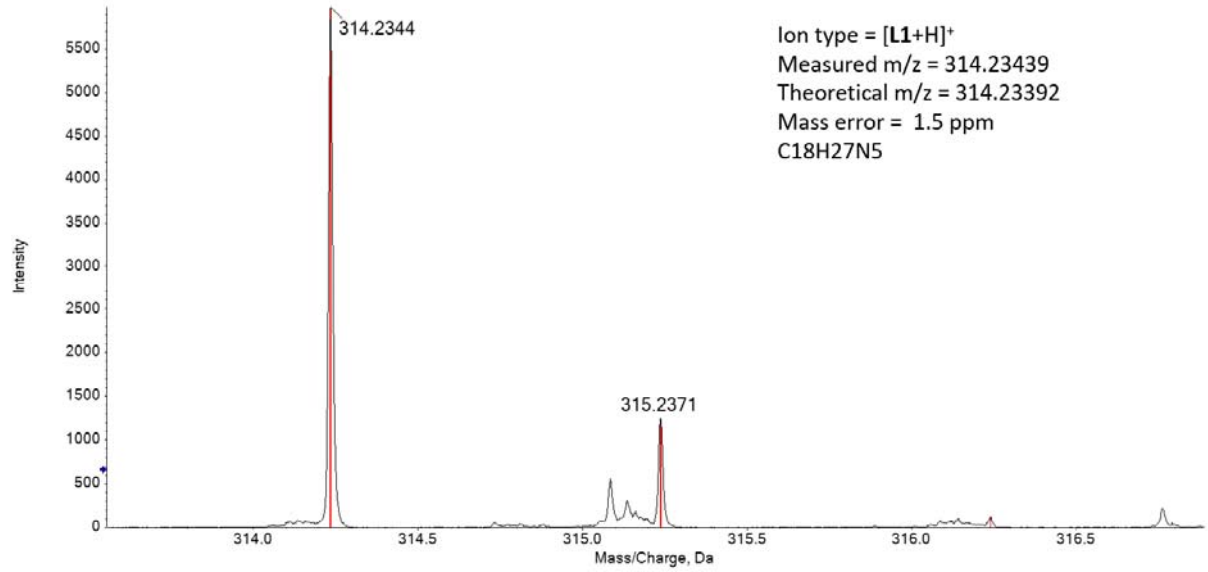

Fig. S18. Isotopic pattern of the [**L1**+H]$^{+}$ (z = 1) ion, with measured (black) and theoretical (red) m/z value of the most abundant isotopic peak, 313.5-317 Da region.

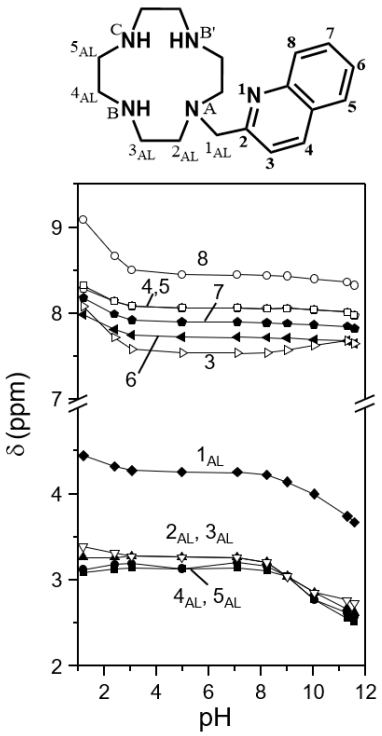

Fig. S19. Plot of the ^{1}H NMR chemical shifts of **L1** as a function of pH.

Table S1: Crystallographic data and refinement parameters for $[(H_4\mathbf{L4})(ClO_4)_4]\cdot 4(H_2O)$.

Empirical formula	$C_{28}H_{46}Cl_4N_6O_{20}$
Formula weight	928.51
Temperature (K)	150
Wavelength (Å)	0.71073
Crystal system, space group	Monoclinic, $P2_1/n$
Unit cell dimensions (Å, °)	a = 14.6135(7) b = 8.3808(4); β = 91.948(4) c = 31.815(1)
Volume (Å^3)	3894.2(3)
Z, Dc (mg/cm^3)	4, 1.584
μ(mm-1)	0.393
F(000)	1936
Crystal size (mm)	0.24x0.22x0.18
θ range (°)	4.213-25.242
Reflections collected / unique	22179/8976
Data / parameters	8976/593

Goodness-of-fit on F^2	1.126
Final R indices [I>2σ(I)]	0.0994/0.1695
R indices (all data)	0.1541/0.1911

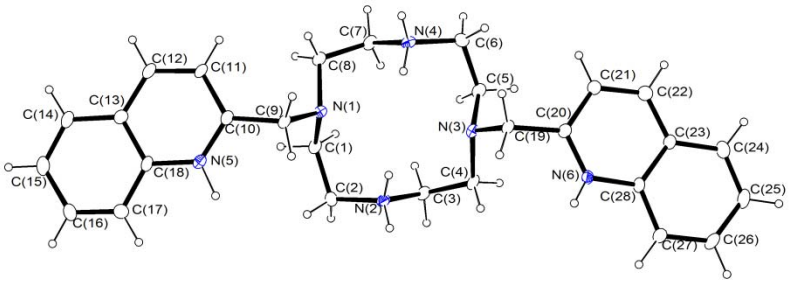

Fig. S20. ORTEP-3 view of the H_4**L4**$^{4+}$ cation in [(H_4**L4**)(ClO_4)$_4$]·4H_2O. Ellipsoids are drawn at the 20% probability.

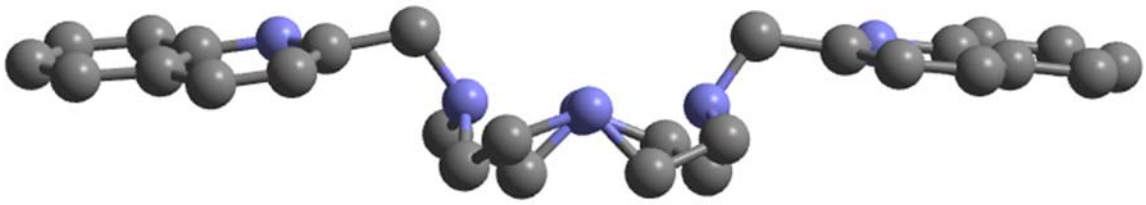

Fig. S21. Ball and sick view of the H_4**L4**$^{4+}$ cation in [(H_4**L**)(ClO_4)$_4$]·4H_2O.

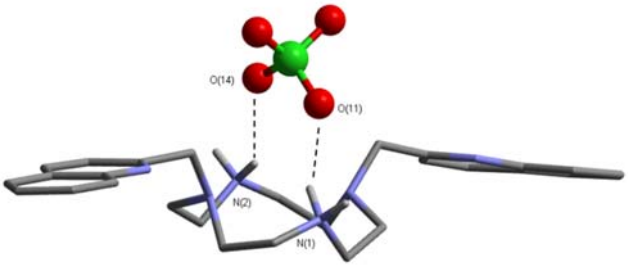

Fig. S22. H_4**L4**$^{4+}$ - ClO_4^- interactions in [(H_4**L4**)(ClO_4)$_4$]·4H_2O.

Table S2. Intra and Intermolecular hydrogen bonds in $[(H_4\mathbf{L4})(ClO_4)_4]\cdot 4H_2O$.

Weak Intramolecular Hydrogen Bonds			
X-H···Y	**X···Y (Å)**	**H···Y (Å)**	**X-H···Y (°)**
N(2)-H(2n2)···N(1)	2.868(6)	2.47(6)	105(4)
N(2)-H(2n2)···N(3)	2.983(6)	2.50(6)	112(4)
N(4)-H(4n2)···N(1)	2.949(6)	2.50(6)	110(4)
N(4)-H(4n2)···N(3)	2.856(6)	2.44(6)	107(4)
Strong Intermolecular Hydrogen Bonds			
X-H···Y	**X···Y (Å)**	**H···Y (Å)**	**X-H···Y (°)**
O(3w)-H(3wa)···O(34a)	3.03(1)	2.31(5)	161(4)
O(3w)-H(3wa)···O(33b)	2.77(5)	2.02(6)	150(4)
N(2)-H(2n1)···O(3w)	2.827(6)	2.00(6)	157(6)
N(2)-H(2n2)···O(11)	2.858(6)	2.09(6)	137(5)
N(4)-H(4n1)···O(4w)	2.782(7)	1.90(6)	168(6)
N(4)-H(4n2)···O(14)	2.883(6)	2.19(6)	131(5)
N(5)-H(5n)···O(1w)	2.740(6)	1.76(6)	173(5)
N(6)-H(6n)···O(2w)	2.774(6)	1.97(6)	172(6)
O(3w)-H(3wb)···O(12)[1]	2.910(6)	2.25(6)	137(5)
O(2w)-H(2wb)···O(13)[1]	2.943(6)	2.19(5)	151(4)
O(1w)-H(1wa)···O(2w)[1]	2.895(6)	2.22(7)	137(3)
O(2w)-H(2wa)···O(3w)[2]	2.813(6)	1.98(4)	173(4)
O(3w)-H(3wb)···O(34b)[2]	2.73(4)	2.10(7)	132(5)
O(1w)-H(1wb)···O(32a)[2]	2.760(9)	2.01(6)	150(5)
O(4w)-H(4wb)···O(24)[3]	2.825(6)	1.99(4)	164(2)
O(4w)-H(4wa)···O(23)[4]	2.965(7)	2.12(4)	170(3)

[1] = -x+1/2+1,+y+1/2,-z+1/2 ; [2] = -x+1/2+1,+y-1/2,-z+1/2 ; [3] = x,+y-1,+z ; [4] = -x+1,-y+1,-z+1

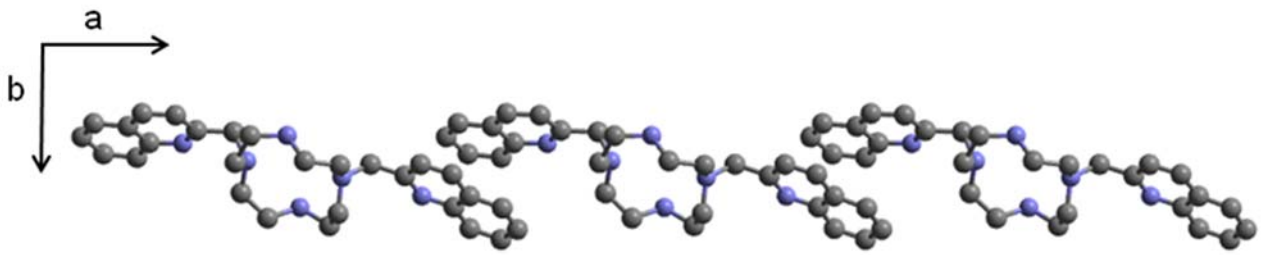

Fig. S23. H_4**L4**$^{4+}$ ribbon in [(H_4**L4**)(ClO_4)$_4$]4·H_2O.

Scheme S1. Fragment searched for in the CSD.

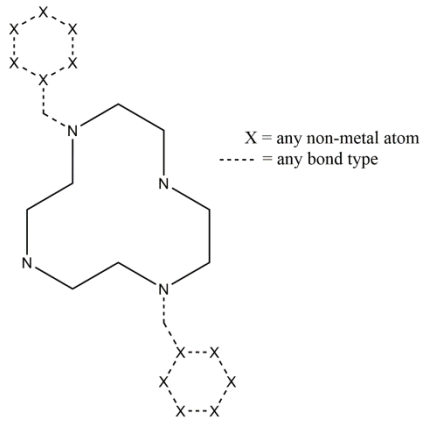

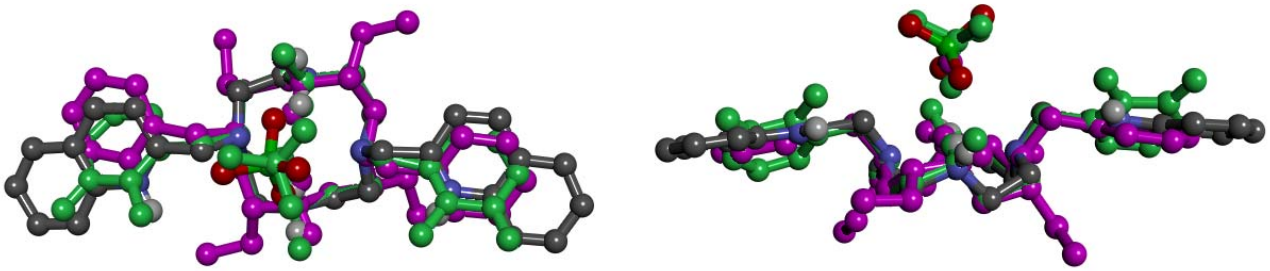

Fig.S24. Superimposition of **1**, HAVFEP (pink) and SELGAT (green). Hydrogen atoms, with the exception of those bonded to nitrogen atoms, have been omitted for clarity.

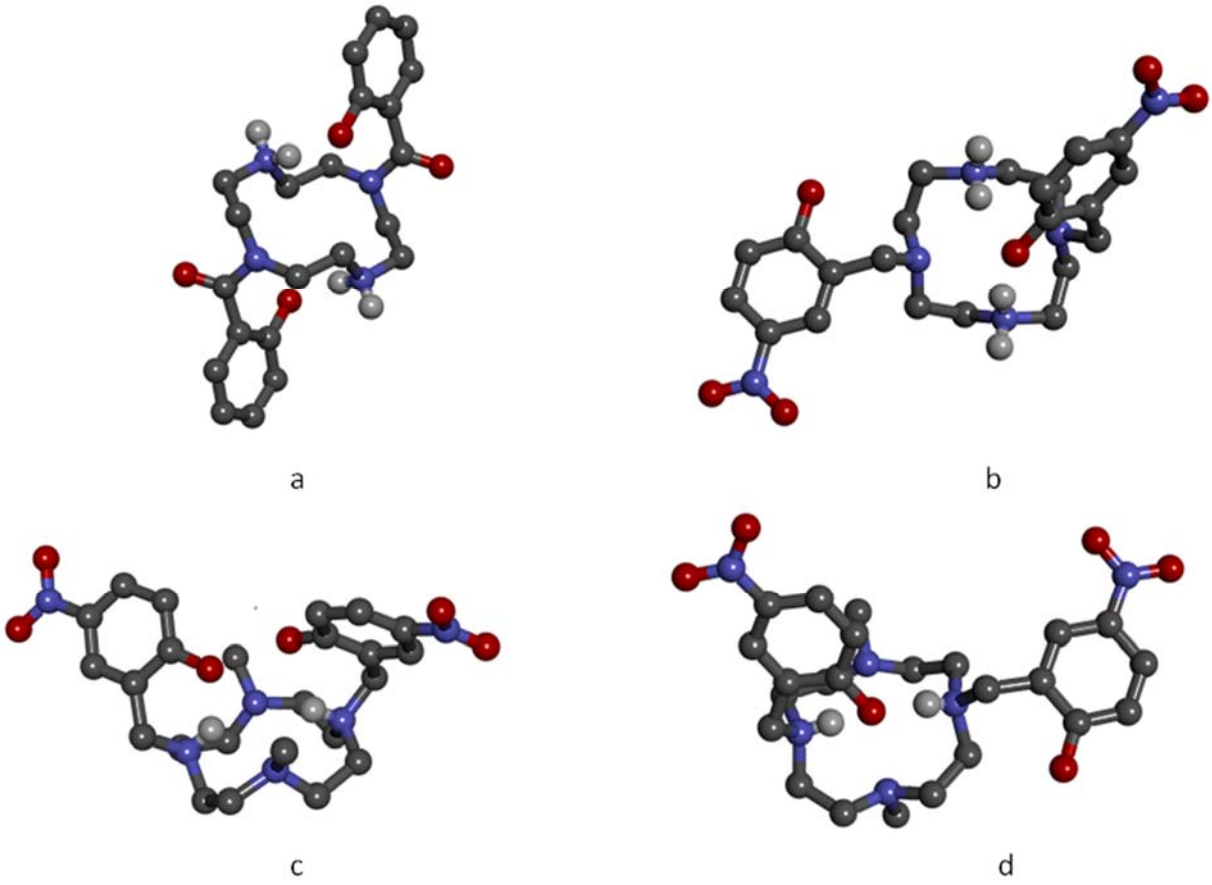

Figure S25. Ball and stick representation of :a) IFIMIU; b) FERBOV; c) LOHXOV; d) LOHXIP.

Table S3. Molar absorption coefficient and fluorescence quantum yield values of the receptors.

	pH	ε (L mol^{-1} cm^{-1}, λ=275 nm)	ε (L mol^{-1} cm^{-1}, λ=316 nm)	Φ (λ_{ex}=295 nm)
L1	2	1755	3030	0.05
	10	2753	1560	0.02
L4	2	1511	3189	0.02
	10	2466	2230	0.02
H_2**L5**	2	922	3029	0.08
	10	1508	1558	0.07

	pH	ε (L mol^{-1} cm^{-1}, λ=313 nm)	ε (L mol^{-1} cm^{-1}, λ=360 nm)	Φ (λ_{ex}=320 nm)
H**L2**	2	3138	1027	0.02
	10	1981	2102	0.05
H**L3**	2	6797	423	-
	10	4529	1931	-

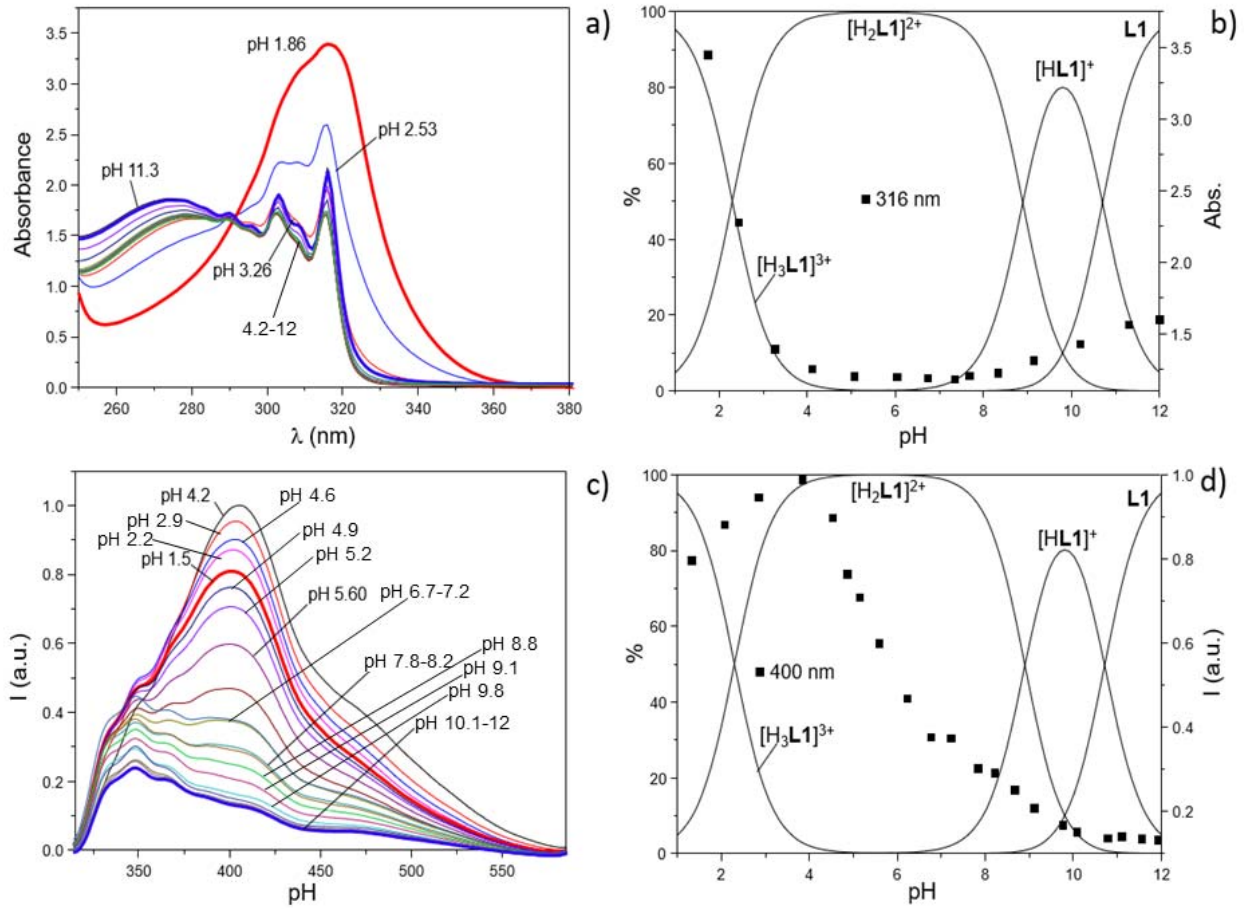

Fig. S26. (a) Absorption spectra of aqueous solutions of **L1** at different pH values and (b) absorbance values at 316 nm (black squares) superimposed to the distribution diagram of the species present in solution ([**L1**] = 5 x 10^{-4} M). (c) Fluorescence spectra of the ligand at different pH values and (d) plot of the fluorescence emission at 400 nm (black squares) superimposed to the distribution diagram of the species present in solution ([**L1**] = 5 x 10^{-4} M, λ_{exc} 316 nm).

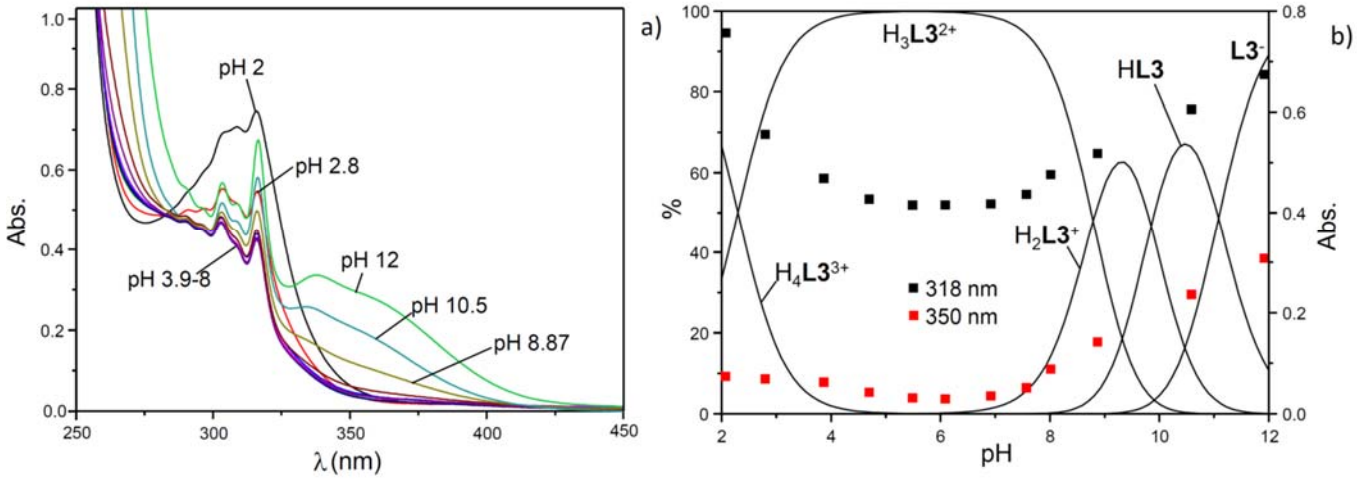

Fig. S27. (a) Absorption spectra of aqueous solutions of H**L3** at different pH values and (b) absorbance values at 316 nm (black squares) and 350 nm (red squares) superimposed to the distribution diagram of the species present in solution ([H**L3**] = 1.5 x 10^{-4} M).

References

[i] CrysAlisPro, Agilent Technologies (2011).

ii CrysAlis RED, Oxford Diffraction Ltd., Version 1.171.pre23_10 beta (release 21.06.2004 CrysAlis171. NET) (compiled Jun 21 2004,12:00:08).

[iii] A. Altomare, G. L. Cascarano, C. Giacovazzo, A. Guagliardi, A. G. Moliterni, M. C. Burla, G. Polidori, M. Camalli, R. Spagna, *J. Appl. Cryst.*, **1999**, *32*, 115.

[iv] Sheldrick, G. M. *SHELX 97*, University of Göttingen, Germany, **1997**.

[v] M. Nardelli, *J. Appl. Cryst*, **1995**, *28*, 659.

[vi] L. J. Farrugia, *J. Appl. Cryst*, **1997**, *30*, 565.

[vii] Macrae, C. F.; Bruno, I. J.; Chisholm, J. A.; Edgington, P. R.; McCabe, P.; Pidcock, E.; Rodriguez-Monge, E.; Taylor, R.; van de Streek; J. Wood, P. A. *J. Appl. Crystallogr*. **2008**, *41*, 466-470.

[viii] Dassault Systèmes BIOVIA, Discovery Studio Visualizer, Release 4.5, San Diego: Dassault Systèmes, 2015.

[ix] Allen F. H. *Acta Crystallogr.* **2002**, *B58*, 380-388.

[x] G. R. Desiraju, T. Steiner, The Weak Hydrogen Bond, Oxford Science Publications, **1999**.

[xi] K. Kobayashi, S. Tsuboyama, K. Tsuboyama, T. Sakurai, *Acta Crystallogr.,Sect.C:Cryst.Struct.Commun.,* **1994**, *50*, 306-312.

[xii] S. Amatori, G. Ambrosi, M. Fanelli, M. Formica, V. Fusi, L. Giorgi, E. Macedi, M. Micheloni, P. Paoli, R. Pontellini, P. Rossi, *J. Org. Chem.,* **2012**, *77*, 2207-2218.

[xiii] a) A. M. Skwierawska, E. Paluszkiewicz, M. Przyborowska, T. Ossowski, *J. Inclusion Phenom.Macrocyclic Chem*., **2008**, *61*, 305-312 (REFCODE = IFIMIU); b) C. V. Esteves, L. M. P. Lima, P. Mateus, R. Delgado, P. Brandao, V. Felix, *Dalton Trans*., **2013**, *42*, 6149-6160 (REFCODE = FERBOV); c) P. Dapporto, V. Fusi, C. Giorgi, M. Micheloni, P. Palma, P. Paoli, R. Pontellini, *Supramol. Chem.*, **1999**, *10*, 243-252 (REFCODES = LOHXIP andLOHXOV)

[IV] Ka-Leung Wong, Jean-Claude G. Bünzli, Peter A. Tanner, Quantum yield and brightness, Journal of Luminescence, Volume 224, 2020, 117256, ISSN 0022-2313, https://doi.org/10.1016/j.jlumin.2020.117256.